

INTEGRATION OF MISSION DESIGN AND NAVIGATION FOR A EUROPA GEODESY ORBITER

Dylan Boone⁽¹⁾ and Daniel J. Scheeres⁽²⁾

⁽¹⁾*H. Joseph Smead Fellow, Aerospace Engineering Sciences, University of Colorado at Boulder
439 UCB, 616-240-0491, dylan.boone@colorado.edu*

⁽²⁾*A. Richard Seebass Chair, Professor, Aerospace Engineering Sciences, University of Colorado at
Boulder 439 UCB, scheeres@colorado.edu*

Abstract: *In this work, we investigate the properties of phase space near a periodic orbit and the applications to orbit design and orbit determination. We compute a low altitude, near-polar periodic orbit and generate an error covariance by processing range-rate and altimetry measurements over seven days. The resulting covariance is used to disperse the orbit initial conditions in a Monte Carlo simulation. We show that the distribution of the Monte Carlo run is biased toward longer orbit lifetimes and that this is due to the stable and unstable manifolds associated with the periodic orbit. We map the orbit determination covariance into manifold coordinates and show that information is preferentially distributed between the acute angle of intersection of the stable and unstable manifolds. Periodic orbit continuation is used to generate a family of orbits with similar phase space characteristics to understand the variation of manifold structure with orbit elements and Jacobi energy. We demonstrate mathematically how the manifold structure of a periodic orbit influences the accumulation of the information matrix in the filtering process and present conclusions regarding the connection between orbit lifetime, orbit design, and orbit determination.*

Keywords: *Europa, phase space, covariance analysis , periodic orbit, orbit determination*

1. Introduction

Orbits about planetary satellites are known to be unstable due to the perturbing gravity of the third body. This effect is dependent on the inclination of the orbit and the strength of the third body's gravity. The goal of the Jupiter Europa Orbiter [3] mission is to measure the Love numbers, geophysical coefficients which give insight into whether there is liquid water on the body . Missions like JEO require near-polar, mapping type orbits which are greatly affected by this gravitational instability. General low altitude, high inclination orbits impact on the surface of the planetary satellite after a time span on the order of weeks [15]. Periodic orbits computed in the Restricted Three Body Problem have the potential to extend this lifetime to the order of months [1].

In this work, we investigate the properties of phase space in the vicinity of a periodic orbit and examine the effect of these properties on the measurement update for orbit determination. Low altitude, near-polar periodic orbits are found in the three-body system at Europa and a seven day initial covariance matrix is created by processing range-rate and altimetry measurement types. This processed covariance is used to draw randomly dispersed initial conditions around the periodic orbit from a multivariate normal distribution in a Monte Carlo analysis. This Monte Carlo simulation shows that there is a preferred nonzero eccentricity for these orbits which can extend the nominal orbit lifetime to around 200 days without control maneuvers.

We employ the concept of manifold coordinates to understand what component of the orbit initial

conditions are along the stable, unstable, and center manifolds associated with the periodic orbit, respectively. We show that the randomly drawn orbits in the vicinity of the periodic orbit exhibit longer lifetimes than the computed periodic orbit. This is shown to be an effect of the stable and unstable manifolds of the periodic orbit. In addition, the relationship between the initial processed covariance of the periodic orbit and the character of dispersed orbits in phase space is discussed. The right eigenvectors of the state transition matrix computed at the system’s periodic time are shown to affect the processing of information in the orbit determination process. We show how the information content of measurements along the stable and unstable manifolds is increased or decreased by the local characteristics of phase space. While these results are computed for the Jupiter-Europa system, any three-body system will exhibit these characteristics to some degree since the mathematical formulation of the problem is the same.

2. Challenges at Europa

2.1. Orbit stability

Geodesy missions generally require low altitude, high inclination orbits for good spatial and temporal coverage of the body under consideration. One issue for the Europa mission is instability due to perturbations on high-inclination orbits from Jupiter’s gravity. The desired low altitude, polar orbits are highly unstable and lead to impact with Europa after several weeks. The inclusion of higher order gravity field harmonics exacerbates the problem and decreases the lifetime of the orbit. The initial NASA description of the mission calls for a one month mapping mission after Europa Orbit Insertion with the possibility of orbit correcting maneuvers. The nominal parameters for the Europa orbit are a 100 km altitude, circular orbit with inclination between 95° and 100° . This high inclination results in a decline of periapse radius due to an increase in the orbit’s eccentricity. This is shown in Figure 1 where the green line shows Europas surface radius which intersects the periapse radius curve after about 22 days. Other studies [2, 20] use this type of orbit in geodesy simulations for a Europa mapping mission but do not discuss the effects of this decay of periapse. Thus, there is a need to evaluate the performance of Europa orbits in terms of orbit lifetime and stability and the measurement precision of desired science parameters.

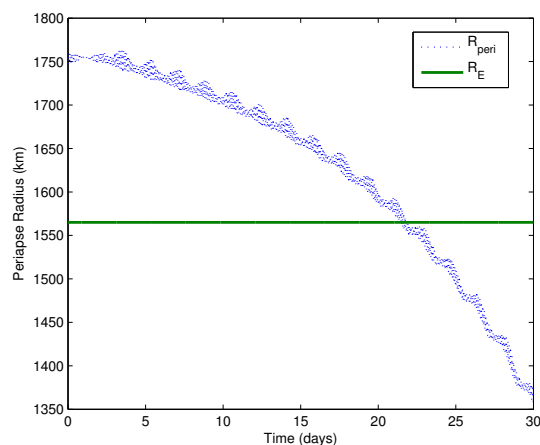


Figure 1. Typical geodesy orbit periapse decay

2.2. Tides and Love numbers

The source of the instability in Europa orbits is the third-body perturbing gravity of Jupiter. This perturbing gravity also raises tides on the surface of Europa. The Love numbers h_2 and k_2 are coefficients of the tide-raising potential which measure the amplitude of the elastic response of a deformed body. Love numbers are dimensionless coefficients and are related to the spherical harmonic expansion of a gravitational potential. Just as the second degree oblateness coefficient of a spherical body will dominate the gravitational perturbation spectrum, the second degree tidal potential and thus the second degree Love numbers dominate tidal perturbations. The h_2 Love number measures the strength of the tidal surface deformation of a body and the k_2 Love number measures the strength of the time-variation in gravitational coefficients [6]. Equation 1 represents the time-variation in the Stokes coefficients as a function of the Love number, the position of Jupiter with respect to Europa, and other system parameters. Equation 2 shows the dependence of radial surface uplift on the h_2 Love number, the surface gravity of the body, and the tidal potential. Through geophysical models, a linear combination of these coefficients serves to constrain the possible ice thicknesses of a Europa with a subsurface ocean [19]. Measurement of these numbers is a primary goal of the JEO mission.

$$\Delta C_{nm} - i\Delta S_{nm} = \frac{k_{nm}}{2n+1} \frac{\mu_J}{\mu_E} \left(\frac{R_e}{r_J}\right)^{n+1} P_{nm}(\sin(\phi)) e^{-im\lambda_J} \quad (1)$$

$$s_R(t) = \frac{h_2}{g_e} \Phi_T \quad (2)$$

3. Jupiter-Europa system model

The specific astrodynamics problem under consideration is the Restricted Three Body Problem (RTBP) at the Jupiter-Europa system. Jupiter and Europa are assumed to be in orbits about their mutual center of mass. The \hat{x} direction points away from Jupiter's initial position on the Jupiter-Europa line, the \hat{z} direction is aligned with the Europa's angular momentum vector, and the \hat{y} direction completes a right-handed coordinate system. A coordinate transformation is used to shift the origin of the coordinate system from the barycenter to Europa's center of mass. Two formulations of the equations of motion are given below. Equation 3 is expressed in an inertial frame centered at Europa and includes the effect of Europa's eccentric orbit about Jupiter. The Jupiter position as seen from Europa is obtained by stepping the true anomaly of Jupiter's orbit and expressing the position in the peri-focal frame, taking the inclination of Europa's orbit to be zero. The gradient of the potential of Europa's extended gravity field is taken in the rotating frame with respect to \vec{r} , the rotating frame position vector, and transformed into the Europa inertial frame using a rotation $R3(\theta)$ about the angular momentum \hat{z} axis. This formulation is used for orbit lifetime integrations and includes the eccentricity of Europa's orbit about Jupiter, the main contribution of

an ephemeris validation run.

$$\ddot{\vec{R}} = -\mu_J \frac{\vec{R} - \vec{R}_{EJ}}{|\vec{R} - \vec{R}_{EJ}|^3} - \mu_J \frac{\vec{R}_{EJ}}{|\vec{R}_{EJ}|^3} - \mu_E \frac{\vec{R}}{|\vec{R}|^3} + R3(\theta)^T \frac{dU}{d\vec{r}} \quad (3)$$

The second formulation of the equations of motion are expressed in the Europa-centered rotating frame where Jupiter and Europa are in circular orbits about their mutual center of mass [17]. The gradient of the potential in this case does not need to be rotated since the partial is taken in the rotating frame. The periodic orbits in this study are converged in the Europa-centered rotating frame with the effects of the higher order Europa gravity terms. Both forms of the equations of motion are non-dimensionalized using the length and time units given in Table 1.

$$\ddot{\vec{r}} = -\mu_J \frac{\vec{r} - \vec{R}_{EJ}}{|\vec{r} - \vec{R}_{EJ}|^3} - \mu_J \frac{\vec{R}_{EJ}}{|\vec{R}_{EJ}|^3} - \mu_E \frac{\vec{r}}{|\vec{r}|^3} - 2n_E \hat{z} \times \dot{\vec{r}} - n_E \hat{z} \times (n_E \hat{z} \times \vec{r}) + \frac{dU}{d\vec{r}} \quad (4)$$

For both forms of the equations of motion, the perturbing potential due to Europa's non-sphericity takes the form of an expansion in associated Legendre polynomials P_{nm} . The gravitational Stokes coefficients C_{nm} and S_{nm} are included in the estimation state or consider lists up to the fourth degree term C_{40} . The numerical values [10] of the nonzero Stokes coefficients used in these simulations are given in Table 1.

$$U = \frac{\mu_E}{r} \sum_{n=0}^N \sum_{m=0}^n \left(\frac{R_e}{r}\right)^n P_{nm}(\sin(\phi)) [(C_{nm} + \Delta C_{nm}) \cos(m\lambda) + (S_{nm} + \Delta S_{nm}) \sin(m\lambda)] \quad (5)$$

Table 1. Europa parameters

Parameter	Value
R_e	1560.8 km
n_E	$2.0483 \cdot 10^{-5}$ rad/s
LU	670900 km
TU	48822.0453055357 s
μ_E	$3202.72 \text{ km}^3/\text{s}^2$
C_{20}	-1041.39 km^2
C_{22}	312.97 km^2
C_{30}	-524117.32 km^3

As discussed in the previous section, the Love number k_2 is tied to variations in the gravitational coefficients. A general expression for these time variations are given in Equation 1. For the second degree coefficients, the k_2 Love number applies to all orders [8]. The complex notation is used to denote that the cosine terms are associated with ΔC_{nm} and the sine terms are associated with ΔS_{nm} . While time variations in the gravity coefficients are necessary for sensing k_2 in the estimation process, care must be taken with C_{20} and C_{22} as both have nonzero time averages. This effectively

changes the nominal value of these coefficients, so the time average component must be subtracted in the dynamics.

4. Periodic orbits

Periodic orbits have the potential to extend orbit lifetime in the unstable environment of the Jupiter-Europa system [7, 12, 4]. In the Europa rotating frame, we search for circular, near polar orbits that make an integer number of revolutions N for every European day ($D = 1$), such that the period of the orbiter is commensurate with the period of Europa's orbit about Jupiter. Equation 6 expresses this number of revolutions N as a function of the orbiter's semi-major axis. Since the Jupiter-Europa semi-major axis a_{EJ} is fixed, we can plot the number of revolutions for different values of spacecraft altitude. Figure 2 below shows the number of Europa revolutions of the orbiter as a function of the orbit altitude. The altitude currently under consideration for a Europa orbiter is 100 km, which corresponds to $N = 41$ in the figure.

$$\frac{N}{D} = \frac{T_E}{T_{sat}} = \sqrt{\frac{\mu_E a_{EJ}^3}{(\mu_J + \mu_E) a_{sat}^3}} \quad (6)$$

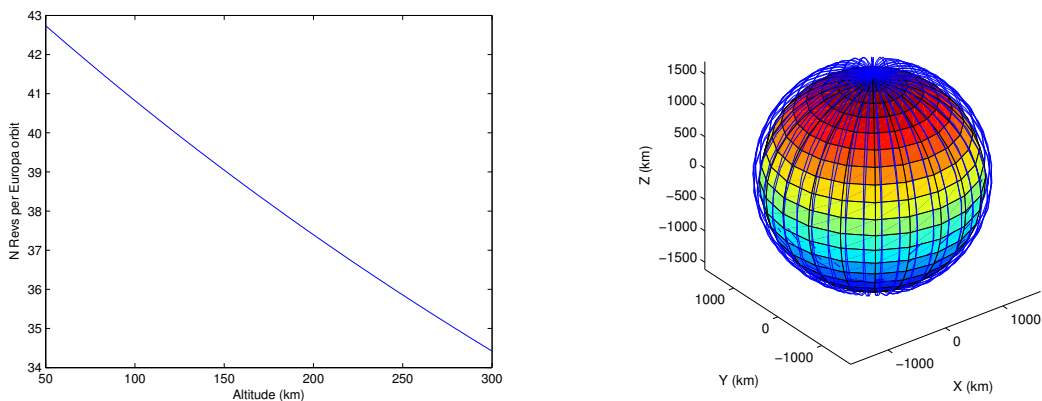


Figure 2. Number of xy-plane crossings per Europa orbit and 97 km altitude periodic orbit

The process for searching out periodic orbits is as follows. First, generate Cartesian initial conditions of the orbit from the chosen orbit elements. We search around the altitude specified by the two-body approximation given above for zero eccentricity, polar orbits by numerically integrating them until the required number of revolutions are completed. This is equivalent to taking a Poincare surface of section as the xy plane and counting the number of crossings until the desired N value is reached. At the N th crossing, the spacecraft state and partials of the Jacobian are used to differentially correct the initial conditions of the orbit to be more periodic using an algorithm given in Scheeres et al [14]. This process is iterated until convergence, which is defined by a user set tolerance of the maximum absolute value of the difference between initial and final states. For the orbit shown here, a tolerance of 1 mm in position and 1 mm/sec in velocity was used. The periodic orbit is also corrected for the

effects of Europa’s non-spherical gravity field. This involves repeating the differential correction procedure subsequently for the C_{20} , C_{22} , and C_{30} gravity coefficients [11]. The final fully converged orbit represented by the orbit elements in Table 2 is used for the Monte Carlo simulation detailed in the following section.

Table 2. Elements for 100 km periodic orbit

Element	Value
a	1658.312 km
e	0.026917
i	90.794°
Ω	0.070868°
ω	274.653°
M	82.277°

5. Covariance analysis

In addition to measuring the tidal Love numbers of Europa for JEO, accurate knowledge of the spacecraft’s position and velocity is necessary for any space mission. We implement a covariance analysis to estimate the accuracy to which the parameters along with Europa’s gravity field are known for this type of mission. The particular implementation is a square-root information filter (SRIF) where the square-root of the information matrix is updated with range and range-rate measurement types.

5.1. Square-root information filter

We use a batch formulation of the square-root information filter to compute an epoch error covariance associated with the orbiter position and velocity, the Europa gravity field coefficients, and the Love numbers. The State Transition Matrix Φ is integrated along with the state and is used to map measurement partials back to epoch. Equation 8 shows the differential equation for the STM which involves the matrix of dynamical partial derivatives A .

$$\Phi(t, t_0) = \frac{\partial \vec{X}(t)}{\partial \vec{X}(t_0)} \quad A(t) = \frac{\partial \dot{\vec{X}}(t)}{\partial \vec{X}(t)} \quad (7)$$

$$\dot{\Phi}(t, t_0) = A(t)\Phi(t, t_0) \quad (8)$$

The measurement types used in this covariance analysis are Earth-centered range-rate and Europa-centered altimetry. The range-rate measurement assumes that Earth is in the direction of the negative x axis for the duration of the simulation, where \vec{R}_{EE} and \vec{V}_{EE} are the Earth position and velocity vectors with respect to Europa. The altimetry measurement includes a time variable surface

deformation s_R due to Jupiter's tidal gravity.

$$\dot{\rho} = \frac{(\vec{r} + \vec{R}_{EE}) \cdot (\vec{v} + \vec{V}_{EE})}{\sqrt{(\vec{r} + \vec{R}_{EE}) \cdot (\vec{r} + \vec{R}_{EE})}} \quad (9)$$

$$h = |\vec{r}| - (R_e + s_R) \quad (10)$$

5.2. Consider parameters

Parameters that effect the estimation process but are not themselves estimated can be considered in the filtering process [18]. An additional consider STM θ is integrated along with the normal STM. The differential equation for this consider STM is shown in Equation 12 and is supplemented with the matrix of dynamical partials with respect to the consider parameter state. For the Europa orbiter, we consider the effect of Jupiter's gravitational parameter, a potential bias in the altimeter measurement, and a potential non-gravitational acceleration constrained to the \hat{z} direction since we are interested in near-polar orbits. This possible non-gravitational acceleration would be due to the sparse atmosphere [9] on Europa but is not implemented in the dynamics. The gravitational coefficients to degree four are also considered. The detailed construction of the SRIF covariance analysis can be found in Boone and Scheeres [1].

$$\theta(t, t_0) = \frac{\partial \vec{X}(t)}{\partial \vec{C}(t_0)} \quad B(t) = \frac{\partial \dot{\vec{X}}}{\partial \vec{C}} \quad (11)$$

$$\dot{\theta}(t, t_k) = A(t) \theta(t, t_k) + B(t) \quad (12)$$

The a priori values for the consider parameters are shown in Table 3. The first value is taken from the uncertainty in Jupiter's mass and the next two are best estimates based on results from published papers on Galileo data [9]. The uncertainty in the gravitational coefficients comes from an initial 7 day SRIF run with coefficients up to J_4 in the estimate list. The third order and higher Stokes gravity coefficients are not included in the dynamics. These values are used in the SRIF consider covariance process for constructing covariance matrices for evaluating periodic orbits at Europa.

5.3. Nominal periodic orbit covariance

Table 4 shows the 1σ state accuracies for a 7-day SRIF covariance run. The position accuracies are on the order of meters and the velocity accuracies are on the order of mm/s. These accuracies may

Table 3. Consider a priori

Parameter	σ
μ_J (km ³ /s ²)	1.001142
a_z (km/s ²)	1×10^{-09}
Δh (m)	100
C_{31}	1.98613×10^{-09}
S_{31}	3.10642×10^{-09}
C_{32}	1.74740×10^{-09}
S_{32}	9.05493×10^{-10}
C_{33}	2.87245×10^{-11}
S_{33}	6.40779×10^{-11}
J_4	2.08224×10^{-07}

be challenging to realize in reality for an outer planet type mission. The gravity field coefficients are very well known with uncertainties four orders of magnitude smaller than the actual non-dimensionalized values used in the dynamics. The Love number accuracies are very good for k_2 which has a nominal value around 0.25 but not tight enough for h_2 which has a nominal value around 1.25 for our simulation.

Table 4. Periodic orbit initial state accuracies

x (km)	1.61287×10^{-04}
y (km)	2.68657×10^{-03}
z (km)	4.06749×10^{-03}
u (km/s)	2.65800×10^{-06}
v (km/s)	5.31885×10^{-07}
w (km/s)	2.44187×10^{-07}
μ_E (km ³ /s ²)	1.75402×10^{-04}
J_2	7.20778×10^{-08}
C_{21}	1.56935×10^{-08}
S_{21}	8.70048×10^{-08}
C_{22}	1.18479×10^{-09}
S_{22}	2.79346×10^{-10}
J_3	5.24517×10^{-06}
k_2	8.61944×10^{-07}
h_2	2.66982×10^{-02}

6. Monte Carlo simulation

To evaluate the statistical properties of an orbit's lifetime, we disperse the initial position and velocity of the orbit by drawing a random vector from the multivariate normal distribution with zero mean and covariance specified by the output of the consider covariance analysis. This process is repeated in a Monte Carlo simulation for 10000 repetitions and the time to impact along with the integrated spacecraft state is saved for each run. Figure 3 shows the eventual decay of the radius magnitude of the nominal 97 km altitude periodic orbit. The left half of Figure 4 shows the lifetime distribution produced by the nominal 7-day covariance applied to a 97 km altitude periodic orbit. The right half of Figure 4 shows the covariance of a generic geodesy type orbit applied to a polar, 100 km altitude orbit. The periodic orbit has an average lifetime of around 83 days, much greater than the 21 day average lifetime of a random geodesy orbit. Neither Monte Carlo simulation produces much variance in their respective lifetime distributions. Investigating this, we scale each term in the periodic orbit's covariance matrix by a factor of 100 in position and velocity to see

the qualitative effect of the distribution. This produces a level of uncertainty of 100's of meters in position and 10's cm/s in velocity that is more realistic for a deep space orbiter.

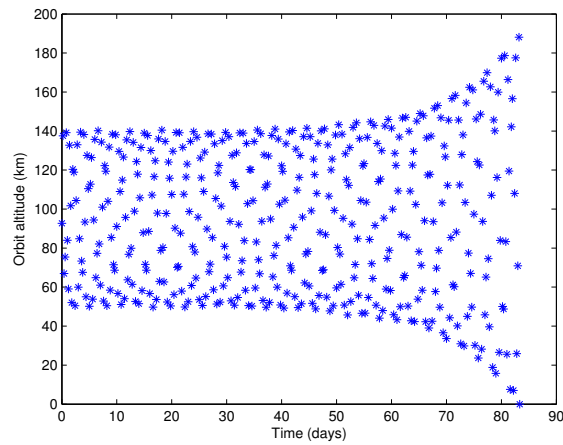


Figure 3. Radius magnitude decay for 97 km orbit

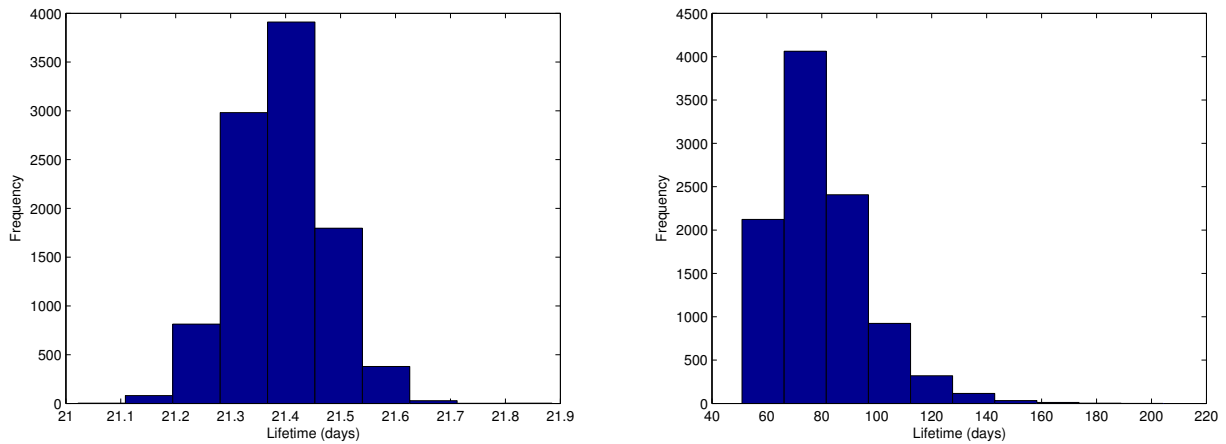


Figure 4. Random geodesy type orbit and 97 km orbit with covariance perturbation scaled

Figure 4 (left) shows the lifetime distribution of a 97 km altitude periodic orbit with initial conditions dispersed by a covariance matrix scaled by factors of 100 in position and velocity. The mean of the distribution is lowered from the nominal 83 days but the distribution is skewed toward greater lifetimes. In addition to this long lifetime bias, none of the orbits dispersed by this augmented covariance matrix reach the 21 day lifetime of a generic polar orbit.

7. Phase space analysis

We seek to find the cause of the increased orbit lifetimes observed in our processed covariance. We examine coordinates other than position and velocity to investigate what is causing the increase in orbit lifetime due to covariance dispersal. Orbit elements are a natural first step. We then implement the concept of dynamic coordinates using the linear stable and unstable manifolds associated with the periodic orbit to determine if information is preferentially distributed along either manifold.

7.1. Orbit element distribution

The initial eccentricity (left) and argument of periapse (right) of the dispersed orbit distribution are shown in Figure 5.

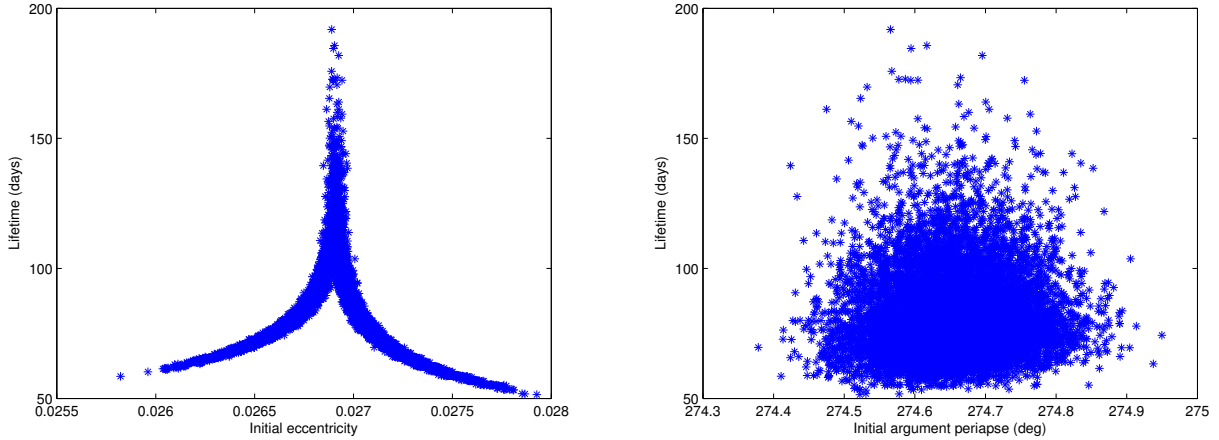


Figure 5. Initial eccentricity dist. (left) Initial argument periapse dist. (right)

There is a definite trend toward a long lifetime eccentricity while the corresponding argument of periapse trend is not as pronounced. We expect orbits in the vicinity of the stable manifold associated with a periodic orbit to have longer lifetimes and that this trend in eccentricity points toward this fact. So, we compute the stable and unstable manifolds of the nominal periodic orbit and project the initial conditions into manifold coordinate space. To do this requires some of the properties of eigenvectors.

7.2. Eigenvectors

Since we expect orbits closer to the stable manifold to exhibit longer lifetimes, we compute the eigenvectors of the State Transition Matrix associated with the stable and unstable manifolds and use them to create a set of local dynamic coordinates associated with these manifolds [5]. A right eigenvector \vec{u} is a column vector that satisfies the property:

$$\Phi\vec{u} = \lambda\vec{u} \quad (13)$$

$$\vec{v}\Phi = \lambda\vec{v} \quad (14)$$

where λ is its associated eigenvalue. A left eigenvector \vec{v} is a row vector which satisfies a similar property. The left eigenvectors of the Monodromy matrix (the STM evaluated at the periodic time T) are used in our manifold coordinate decomposition computation due to the orthogonality properties of left and right eigenvectors.

$$\vec{v}_i \cdot \vec{u}_j = \begin{cases} 1, & \text{if } i = j. \\ 0, & \text{if } i \neq j. \end{cases} \quad (15)$$

From Equation 15, all left eigenvectors are orthogonal to all right eigenvectors except for those pairs generated with the same eigenvalue. So, the left stable eigenvector is orthogonal to all right eigenvectors except the right stable eigenvector. Unstable manifolds are characterized by the eigenvector paired with an eigenvalue with magnitude greater than one. Likewise, a stable manifold is characterized by the eigenvector paired with an eigenvalue with magnitude less than one.

7.3. Manifold coordinates

The STM is integrated in the rotating frame of the Restricted Three Body Problem and evaluated at Europa's repeat period of 3.55 days. Since the Monte Carlo lifetime runs are conducted in the inertial frame for realism, the state must be transformed back to the rotating frame for this computation. The manifold coordinates a_u and a_s representing the unstable and stable components of the state are computed by taking the dot product of the left unstable \vec{v}^u and left stable \vec{v}^s eigenvectors with the difference between the dispersed state and the periodic orbit state as in Equations 17.

$$\begin{aligned} \delta\vec{x} &= (\vec{X}_{disp} - \vec{X}_{PO}) \\ \vec{\alpha} &= \text{real}(\vec{v}^c) \\ \vec{\beta} &= \text{imag}(\vec{v}^c) \end{aligned} \quad (16)$$

The representation of the center manifold includes a magnitude and a phase difference since the center eigenvalues have imaginary components. The left eigenvectors are normalized to have magnitude one while the orbiter state difference retains its magnitude. The orbiter states are non-dimensionalized as both the STM and state are integrated using non-dimensional equations of motion.

$$\begin{aligned} a_u &= \vec{v}^u \cdot \delta\vec{x} \\ a_s &= \vec{v}^s \cdot \delta\vec{x} \\ \rho &= \left[(\delta\vec{x}^T \vec{\alpha})^2 + (\delta\vec{x}^T \vec{\beta})^2 \right]^{1/2} \\ \gamma &= \text{atan}(\delta\vec{x}^T \vec{\beta} / \delta\vec{x}^T \vec{\alpha}) \end{aligned} \quad (17)$$

Taking the difference between the nominal periodic orbit state and the dispersed initial conditions from the Monte Carlo simulation, we obtain the results in Figure 6. We choose to project the

stable and unstable manifold coordinates into the plane of intersection of the six-dimensional stable and unstable manifolds. The red and green solid lines represent the unstable and stable manifolds respectively. The x and y coordinates of the charts are chosen such that the x -axis bisects the acute angle of intersection of the stable and unstable eigenvectors. The projections of the manifold coordinates are color coded based on the lifetime of the dispersed orbits. Blue denotes orbits with lifetimes greater than 50 but less than 70 days, cyan denotes lifetimes greater than 70 but less than 100 days, magenta denotes lifetimes greater than 100 but less than 150 days, and the zoomed in chart (right) includes yellow-marked orbits with greater than 150 days lifetime.

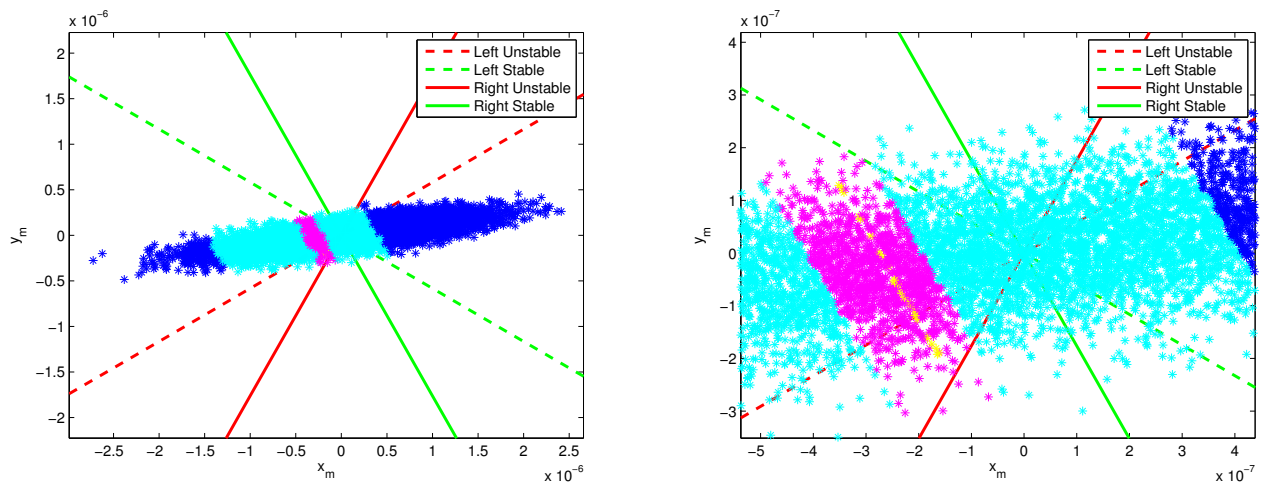


Figure 6. Dispersed orbit dynamic coordinate projection distribution (left) and zoom (right)

The distribution is slightly aligned toward the left unstable eigenvector and the longer lifetime orbits are slightly aligned with the left stable eigenvector. The critical result comes from the properties of left and right eigenvectors. The left stable eigenvector (corresponding to the stable manifold) is orthogonal to all other right eigenvectors of the Monodromy matrix except the right stable eigenvector. Similarly, the left unstable eigenvector is orthogonal to all right eigenvectors besides the right unstable eigenvector. In our projection, the right stable eigenvector is perpendicular to the left unstable eigenvector. It is likely that the orbits along the line formed by the yellow longest lifetime orbits in the distribution are aligned with the right stable eigenvector. When mapping forward in time, orbits aligned with the stable manifold approach the periodic orbit and orbits aligned with the unstable manifold depart from the periodic orbit. The long lifetime orbits produced by the covariance dispersal follow the stable manifold toward the periodic orbit and then depart along the unstable manifold, effectively doubling the nominal lifetime of 83 days to greater than 150 days.

Figure 7 shows the manifold coordinate distribution for inertial integrations with Europa eccentricity set to zero. The lifetime distribution is similar in character to the eccentric integrations with the main difference being the longer lived orbits are much closer to the stable manifold. This is logical since this situation is closer to the Restricted Three Body Problem.

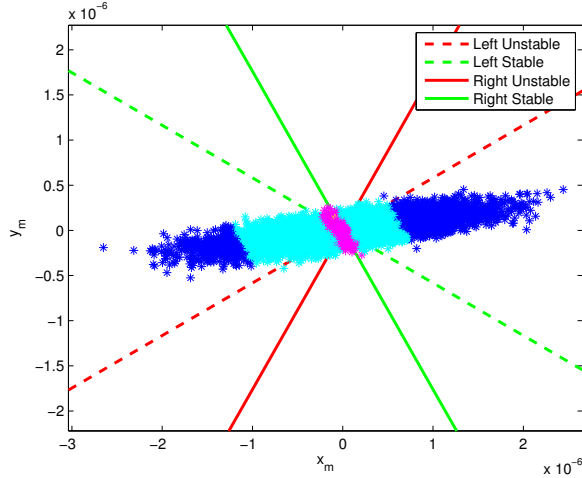


Figure 7. Dispersed orbit dynamic coordinate projection distribution without eccentricity

7.4. Families of periodic orbits

The manifold structure described above is valid only for that particular nominal periodic orbit. In this section we continue this periodic orbit by varying the Jacobi energy to find new periodic orbits and compare their eigenvalues, periods, and orbit elements. Small steps in Jacobi energy are required to continue the orbit within its same family. The algorithm for this process is given in Appendix B. We use the same Poincare map of $z = 0$ and iterate the new periodic orbit to convergence using the same method as the original computation. The derivation of the correction to the initial state for continuation follows.

This process of continuing a family of periodic orbits is applied to the nominal periodic orbit considered with 1000 steps of $\delta C = 10^{-6}$ in the positive and negative energy directions. This process converges uniformly with the average difference in Jacobi energy of the newly converged orbit $\delta C = 1.7 \cdot 10^{-6}$. The characteristics of the nominal periodic orbit and the longest lifetime orbit from the Monte Carlo covariance draw are shown in Table 5. The difference in Jacobi energy is on the order of 10^{-4} and the resulting eigenvalues of the Monodromy matrix and angles θ between the stable and unstable manifolds are nearly identical, varying only in the 6th decimal for eigenvalues.

Table 5. Orbit characteristics

	C	θ	λ_u	λ_s
Original PO	568.429284148851	60.4064545899096	1.29157375506888	0.77424924146563
191 day LL orbit	568.429370877893	60.4090207414058	1.29157565987339	0.774248099609874

The left side of figure 8 below shows the decrease in orbit period resulting from a change in Jacobi energy from continuing the periodic orbit family. The right side of that figure shows changes in the eigenvalues of the Monodromy matrix, with most of the change occurring in the complex eigenvalues associated with the center manifold. The near-unity real eigenvalues are maintained through the continuation process as are the stable ($\lambda < 1$) and unstable ($\lambda > 1$) real eigenvalues. The variation in the complex eigenvalues is on the order of 10^{-5} .

The decrease in orbit period shown in Figure 8 suggests that the continued orbits are faster in some

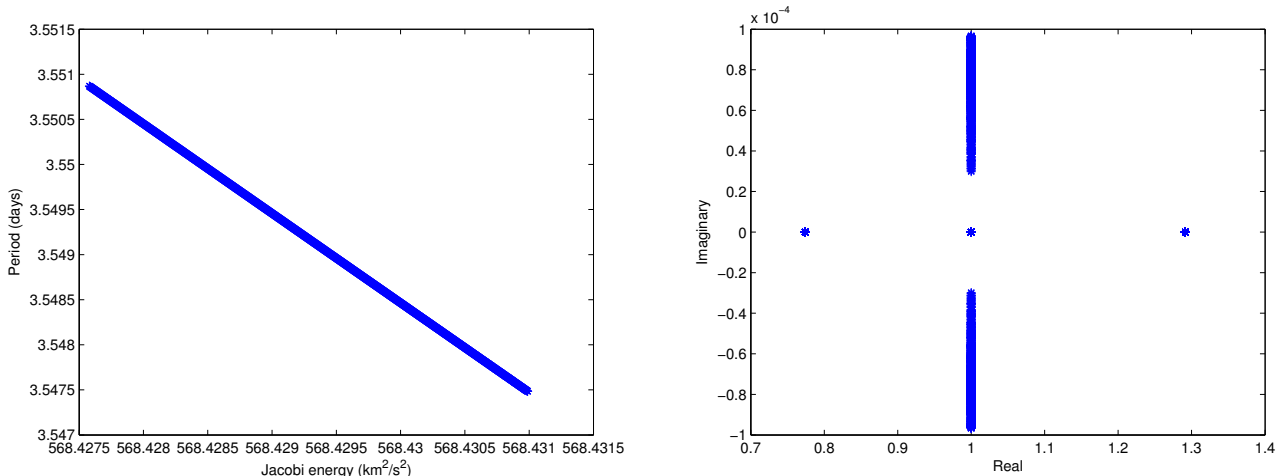


Figure 8. Change in orbit period with energy (left) and eigenvalue evolution (right)

sense than the nominal periodic orbit. Since the number of Europa revolutions per orbit about Jupiter is conserved ($N = 41$), the semi-major axis should decrease. This is observed in the orbit elements shown in Figure 9 where the semi-major axis decreases and the eccentricity increases with the increase in Jacobi energy. The left side of the figure shows that the inclination and argument of periapse also decrease with the increase in Jacobi energy. So, while the eigenstructure of the Monodromy matrix is basically conserved in the continuation process, the resulting continued periodic orbits have slightly different orbital elements. Orbit eccentricity increases slightly but remains near the optimal long lifetime value.

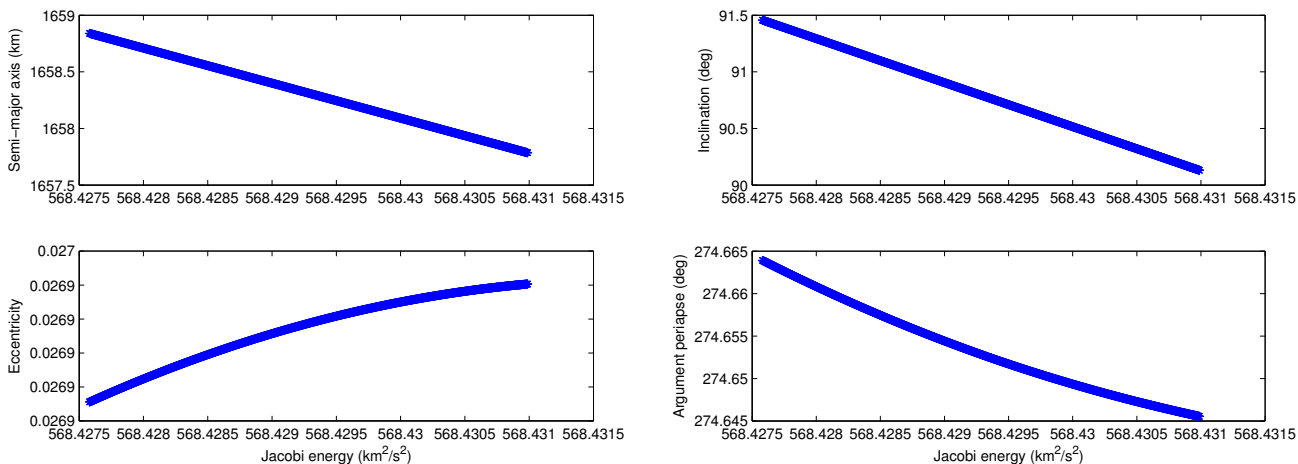


Figure 9. Changes in periodic orbit elements with continuation

Figure 10 shows the eigenstructure of the iteration with an increase in energy of 10^{-3} above that of the nominal periodic orbit. As the eigenvalues of the continued orbits changed very little, so too does the manifold coordinate distribution change very little for this continued orbit. The yellow line formed by the longest lifetime orbits of the distribution shifts slightly to the left but the overall structure of this decomposition is preserved. The right side of the figure shows the magnitude and phase of the center manifold components of the dispersed orbits. The phase of the center manifold

coordinate shows that the majority of the dispersed orbits are either in phase or antiphase with the center manifold, either at 0° or -180° . Only 10 out of the 35 longest lifetime orbits (> 150 days lifetime) are antiphase with the longest lifetime orbit being in phase.

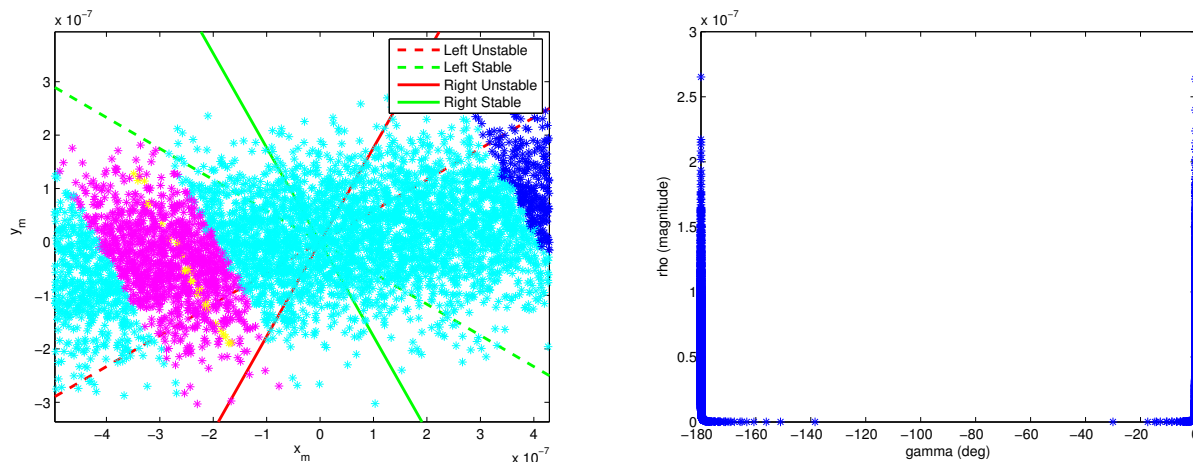


Figure 10. Periodic orbit structure with $\delta C = 10^{-3}$ off nominal

This continuation process shows that the longer lifetime dispersed orbits have manifold structures very similar to that of the nominal periodic orbit. This makes sense since the difference in Jacobi energy between the nominal and longest lifetime dispersed orbit is small relative to the original value ($10^{-5}\%$). This analysis shows that the orbit determination covariance contains a family of periodic orbits and their associated structures. The covariance draw samples across this family with similar manifold characteristics and is not controlled by any one particular periodic orbit.

7.5. Numerical accuracy

We expect that trajectories falling on or near the right stable manifold will have desirable lifetime properties. Orbit initial conditions constructed using an extension of the linear right stable manifold should have comparable lifetimes to our Monte Carlo distribution. We take the longest lifetime orbit from our Monte Carlo orbit simulation and disperse it in small increments along the right stable manifold. Since the long lifetime orbits from our simulation have manifold coordinates up to 10^{-7} , we disperse in increments of $\epsilon = 10^{-9}$ up to 10^{-7} along either extent of the stable manifold, resulting in 201 trajectories. We take the $z = 0$ surface of section and decompose the resulting points into manifold coordinates. This integration is carried out 100 days backward in time and a representative trajectory is shown in Figure 11. The manifold coordinates themselves circulate and repeat about every 3.55 days which is the system repeat period for Europa about Jupiter. The general trend carries the trajectories slightly off the stable manifold but every 3.55 days or $N = 41$ revolutions, the coordinate decomposition falls on or nearly on the stable manifold again.

As a check on our numerical accuracy, we integrate backward and then forward along the stable manifold amounts of time corresponding to multiples of the system repeat period and compare the resulting state with the initial condition. This is shown in Figure 12. The magnitude of the position and velocity deviations are plotted against the number of full system repeat periods. The numerical

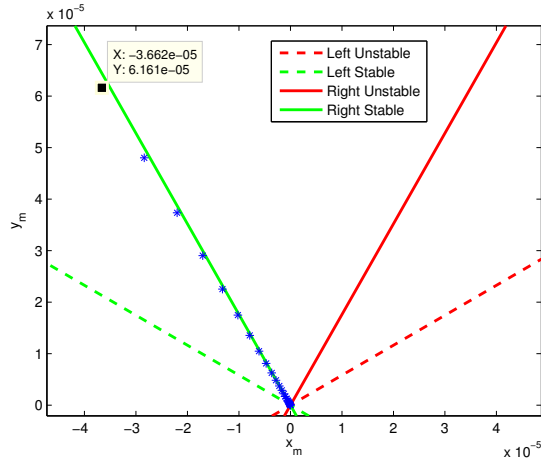


Figure 11. Integration back in time $z = 0$ manifold coordinates and integration error

error is approximately linear up until around 20 repeat periods and then changes to a quadratic character. We may be able to obtain better accuracy along the stable manifold with a higher order integrator, such as an RK78 as opposed to the RK 45 used here.

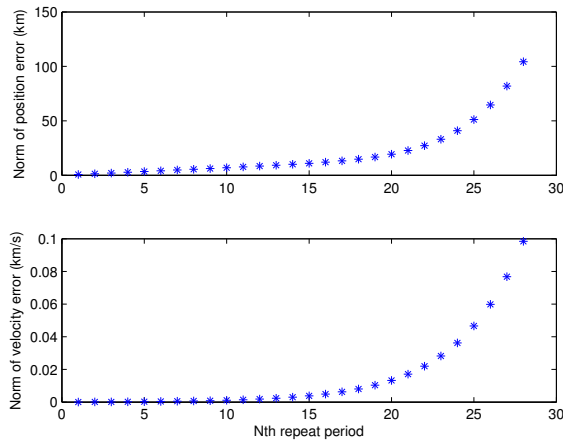


Figure 12. Integration error along the stable manifold

Since the points which occur at multiples of the system repeat period fall back on the stable manifold, we use them as initial conditions for forward integration. Starting near the fixed point origin, we take each trajectory return on the stable manifold and integrate it forward in time until impact with the surface. The orbit lifetimes for integration of these points on or near the stable manifold are shown in Figure 13. Interestingly, the trajectory closest to the fixed point does not give the longest lifetime. The longest lifetime orbit achieved from this process is generated by the 25th full system repeat point on the stable manifold. This point is called out as a data point on Figure 11. The lifetimes peak with this 25th repeat point which corresponds closely to the change in character of the error associated with integrating along the stable manifold. However, the maximum lifetime found this way is less than the original long lifetime orbit found in the Monte Carlo simulation: 162 days compared to 191 days. Both choosing an orbit based on its alignment with the stable manifold

and choosing the longest lifetime orbit from a covariance dispersion of a periodic orbit yield similar lifetimes with the longer lifetime orbit found in our covariance dispersal.

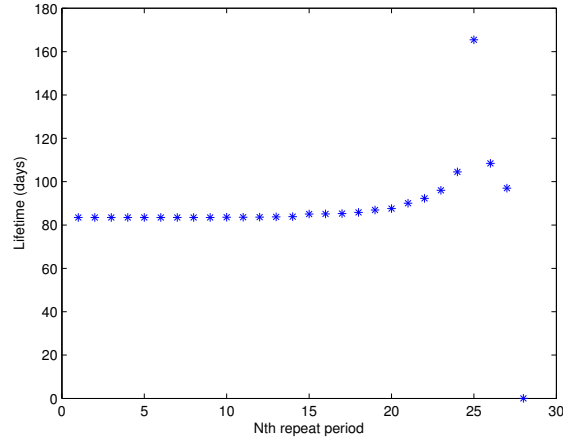


Figure 13. Forward integration orbit lifetime

8. Influence on information matrix

Now we consider the information matrix used in the orbit determination process for estimating the orbiter position and velocity as well as any desired science or system parameters. The measurement partials accumulated in this process are mapped by the STM and are influenced by the properties of its eigenvectors. We demonstrate how information from a particular measurement is either increased or decreased based on the stable and unstable manifolds associated with a periodic orbit and make a connection between this information mapping and the observed Monte Carlo lifetime distribution.

8.1. Structure of the information matrix

In a batch formulation of the square-root information filter, the information matrix Λ is updated with each processed measurement via the measurement partials \tilde{H} . These measurement partials are mapped to the epoch state by means of the STM which is integrated along with the equations of motion. The update is as follows:

$$\Lambda' = \Lambda + \Phi^T(t, t_0) \tilde{H}^T \tilde{H} \Phi(t, t_0) \quad (18)$$

The STM can be decomposed into a product of matrices of right eigenvectors, eigenvalues, and left eigenvectors.

$$\Phi = ULV^T = [\vec{u}_1 \ \vec{u}_2 \ \dots \ \vec{u}_n] \begin{bmatrix} \lambda_1 & & 0 \\ & \ddots & \\ 0 & & \lambda_n \end{bmatrix} \begin{bmatrix} \vec{v}_1 \\ \vec{v}_2 \\ \vdots \\ \vec{v}_n \end{bmatrix} \quad (19)$$

The Monodromy matrix is the State Transition Matrix evaluated at a time equal to the system's period. We can choose to decompose the measurement partial into components along the left eigenvectors of the Monodromy matrix since these vectors span the measurement space. Using as many as are necessary to represent the particular partial:

$$\tilde{H} = c_i \vec{v}_i^T \quad (20)$$

Decomposing the state transition matrix and the measurement partials using the eigenvalues and eigenvectors of the Monodromy matrix, we have the information matrix update equation:

$$\Lambda' = \Lambda + VLU^T (c_i \vec{v}_i) (c_i \vec{v}_i^T) ULV^T \quad (21)$$

where U is a matrix of right eigenvectors \vec{u}_i and V is a matrix of left eigenvectors \vec{v}_i . Using the properties of left and right eigenvectors, we can simplify this update relationship. The dot product of a left eigenvector and right eigenvector is 0 unless their indices are equal. In other words, all left and right eigenvectors are orthogonal to one another except for those paired with the same eigenvalue.

$$\vec{v}_i \cdot \vec{u}_j = \begin{cases} 1, & \text{if } i = j. \\ 0, & \text{if } i \neq j. \end{cases} \quad (22)$$

Using this property, only the eigenvector(s) aligned with the particular measurement partial will contribute to the addition to the information matrix. Using the matrix exponential form of the STM, where σ_i is the eigenvalue of the dynamics partials matrix A corresponding to λ_i :

$$\Lambda' = \Lambda + \vec{v}_i e^{\sigma_i t} (c_i \vec{u}_i^T \vec{v}_i) (c_i \vec{v}_i^T \vec{u}_i) e^{\sigma_i t} \vec{v}_i^T \quad (23)$$

$$= \Lambda + c_i^2 e^{2\sigma_i t} \vec{v}_i \vec{v}_i^T \quad (24)$$

Since the batch formulation of the SRIF references the epoch time, all subsequent measurements will be mapped backward in time. The unstable manifold direction has a positive real eigenvalue λ greater than one. So its natural logarithm is positive and the measurements aligned with the unstable manifold direction will be mapped according to the exponential $e^{\sigma t}$ and will increase the amount of information in Λ .

8.2. Measurement mapping

The longest lifetime orbits from the initial condition distribution plots in the previous section are aligned with the right stable manifold direction: parallel and offset. The entire distribution regardless of orbit lifetime is perpendicular to this right stable manifold direction with the delineations in orbit lifetime parallel to this same vector. The smallest axis of the covariance ellipsoid falls between the acute angle of intersection of the right stable and unstable manifolds. This corresponds to the area of greatest information density since the information matrix and covariance matrices share an inverse relationship. The bottom branch of long lifetime orbits falls within this area of concentrated information while the top branch lies just on the obtuse side of the manifold intersection.

We examine the properties of linear manifolds according to dynamical systems theory in order to explain the orientation of the covariance distribution and the increase in lifetimes of the dispersed orbits. Propagating trajectories forward in time along the stable manifold generally results in contraction in state uncertainty and propagating along the unstable manifold results in an expansion of uncertainty [16]. Similarly, propagating backward in time reverses these relationships; the stable manifold expands and the unstable manifold contracts orbit knowledge. In the epoch formulation of our SRIF filter, all measurements are mapped back to the initial time. As we demonstrated mathematically, a measurement along the unstable manifold mapped back in time will result in an expansion of its information content, causing the direction of the unstable manifold at epoch to be more well known. Likewise a measurement along the stable manifold mapped back in time will cause a contraction in information content and the stable direction will be less well known at epoch. Measurements partials which fall within the acute angle of manifold intersection will be mapped toward the fixed point origin along the unstable and away along the stable when mapping back to epoch. The same process occurs for other measurement partials outside this region but the same amount of information is more concentrated inside the acute intersection area. Thus, the greatest extent of the overall covariance distribution lies in the obtuse intersection areas while the smallest extent falls within the acute intersection areas. Since the measurement partials will in general be distributed randomly in manifold space, the same information in the obtuse region is compressed into a much smaller area in the acute area. This results in smaller uncertainty for this region. The long lifetime orbits bisect the small axis of the covariance distribution and it may be the eccentricity of Europa's orbit which moves these orbits farther from the periodic orbit in manifold coordinates.

9. Conclusions

In this work, we present orbits dispersed from a periodic orbit initial condition using a processed error covariance and study their properties in phase space using lifetime integration and manifold coordinate decomposition. The longest-lifetime orbits from this dispersion are shown to be aligned

with the right stable manifold associated with the nominal periodic orbit. Additional periodic orbits continued in the same family as this periodic orbit have similar manifold structures although the orbit period and semi-major axis decrease with increasing Jacobi energy. The lifetime distribution of the dispersed orbits has its smallest axis aligned with the long lifetime orbits, corresponding to the area of greatest information density. We connect this observation to the orbit determination process via the structure of the information matrix. We show mathematically how the structure of the information matrix is influenced by the manifold structure of a periodic orbit. Measurements along the unstable manifold are mapped back in time to epoch resulting in an increase information or a decrease in the uncertainty of the desired measurement. Likewise, measurements along the stable manifold mapped forward in time give better estimation uncertainties. This is useful for obtaining knowledge of the orbiter state at times subsequent to the measurement. As a check on our Monte Carlo simulation we construct orbits along the stable manifold and compare the lifetimes to our covariance distribution. Orbits directly along the stable manifold have longer lifetimes than random geodesy type orbits but do not match the longest lifetime orbits from the covariance orbit dispersion.

We have observed long lifetime orbits present within the error covariance from the orbit determination process. This covariance has information which is preferentially distributed according to the stable and unstable manifolds of a periodic orbit. We show this by mapping the orbit determination covariance into manifold coordinates and discussing how measurements are mapped in time according to the State Transition Matrix's eigenvectors. These long lifetime orbits are an unexpected benefit of conducting simultaneous orbit determination and orbit design. A next step for this work will be applying the manifold coordinate decomposition to different measurement types and schedules in the orbit determination process to determine preferential science measurement methods from an information matrix standpoint.

10. References

- [1] Boone and Scheeres. "Evaluating periodic orbits for the JEO mission at Europa in terms of lifetime and stability." AAS Astrodynamics Specialist Conference 2011, Girdwood, AK. AAS 11-518.
- [2] Casotto and Padovan. "Detecting Body Tides and Librations of Europa with an Altimetric Exploration Mission." AIAA/AAS Astrodynamics Specialist Conference. Hawaii, August 2008.
- [3] Clark, Magner, et al. "Jupiter Europa Orbiter Mission Study 2008: Final Report." NASA Outer Planet Flagship Mission Reports. Posted: Feb. 12, 2009.
- [4] Gomez, G., Lara, M., Russell, R., "A Dynamical Systems Approach to the Design of the Science Orbit around Europa, Paper ISTS 2006-d-02, 19th International Symposium on Space Flight Dynamics, Kanazawa, Japan, Jun 2006.
- [5] Gustafson and Scheeres. "Dynamically relevant local coordinates for halo orbits." AAS Astrodynamics Specialist Conference 2008.
- [6] Lambeck, K. *Geophysical Geodesy: The Slow Deformations of the Earth*. Clarendon Press. Oxford 1988.

- [7] Lara, M., Russell, R.P., “On the Design of a Science Orbit about Europa”, Paper AAS 06-168, presented at the AAS/AIAA Space Flight Mechanics Meeting. Tampa, Florida, 2006.
- [8] McCarthy, D. (ed.) IERS Conventions (1996), IERS Technical Note 21, International Earth Rotation Service, Observatoire de Paris, July 1996.
- [9] McGrath et al. “Observations of Europa’s Tenuous Atmosphere” in *Europa*. University of Arizona Press, Tuscon, 2009.
- [10] Paskowitz-Possner, Marci. *Orbit Design and Control of Planetary Satellite Orbiters in the Hill 3-Body Problem*. Dissertation, PhD Aerospace Engineering, University of Michigan-Ann Arbor, 2007.
- [11] Paskowitz-Possner and Scheeres. “Design of Science Orbits about Planetary Satellites: Application to Europa. JGCD 29(5): 1147-1158, 2006.
- [12] Russell, Ryan P. “Global Search for Planar and Three-Dimensional Periodic Orbits Near Europa.” AAS 05-290.
- [13] Scheeres, D.J. *Orbital Motion in Strongly Perturbed Environments: Applications to Asteroid, Comet and Planetary Satellite Orbiters*. Springer, 2012.
- [14] Scheeres et al. “Evaluation of the Dynamic Environment of an Asteroid: Applications to 433 Eros”. JGCD 23(3): 466-475, 2000.
- [15] Scheeres et al. “Stability Analysis of Planetary Satellite Orbiters: Application to the Europa Orbiter. JGCD 24(4): 778-787, 2001.
- [16] Scheeres, Han, and Hou. “Influence of Unstable Manifolds on Orbit Uncertainty.” JGCD 24(3): 573-585, 2001.
- [17] Szebehely, V. *Theory of Orbits: The Restricted Problem of Three Bodies*. Academic Press, 1967.
- [18] Tapley, Schutz, and Born. *Statistical Orbit Determination*. Elsevier Academic Press, 2004.
- [19] Wahr et al. “Tides on Europa, and the thickness of Europa’s icy shell.” JGR 111(E1), 2005.
- [20] Wu et al. “Probing Europas Hidden Ocean from Tidal Effects on Orbital Dynamics. GRL 28(11): 2245-2248, 2001.